RESEARCH ARTICLE
SPACE PHYSICS

Earth and Planetary Physics
10: 280–290, 2026
doi: 10.26464/epp2026030

On the dominant mechanisms of ion energization in collisionless plasma turbulence

QianYun Xu[1,2], Meng Zhou[1,2*], ZhiHong Zhong[1,2], Ye Pang[2], and XiaoHua Deng[2]

[1]Department of Physics, School of Physics and Materials Science, Nanchang University, Nanchang 330031, China;

[2]Institute of Space Science and Technology, Nanchang University, Nanchang 330031, China

Key Points:

- Ions are primarily energized through the diamagnetic drift in the magnetosheath turbulence.
- Ion energization predominantly occurs around the ion inertial scales and on a larger scale than electrons.
- The relationship between ion energization/heating and coherent structures remains unclear and requires further research.

Citation: Xu, Q. Y., Zhou, M., Zhong, Z. H., Pang, Y., and Deng, X. H. (2026). On the dominant mechanisms of ion energization in collisionless plasma turbulence. *Earth Planet. Phys.*, *10*(2), 280–290. http://doi.org/10.26464/epp2026030

Abstract: Turbulence is ubiquitous in space and astrophysical plasmas, and it plays a crucial role in energy dissipation and plasma energization. However, the exact mechanism for particle energization in turbulent plasma is not fully understood. This study utilizes a fluid framework, which does not rely on the guiding-center approximation, to quantitatively analyze ion energization in turbulence by using observational data from the Magnetospheric Multiscale Mission (MMS) in the Earth's magnetosheath, revealing the dominant role of the diamagnetic drift in ion energization. This research further demonstrates that ion energization occurs concentrated around the ion inertia length. However, in contrast to electrons, the relationship between ion energization/heating and coherent structures remains unclear and requires further research. This study provides new perspectives for understanding turbulent energy dissipation and particle heating.

Keywords: turbulence; magnetosheath; ion energization

1. Introduction

Turbulence plays an essential role in space and astrophysical plasmas, where energy dissipation and particle heating are central to understanding plasma dynamics. In turbulent plasmas, energy is transferred from large scales (e.g., fluid scales) to kinetic scales (e.g., ion and electron inertial lengths), where energy dissipates, leading to plasma heating and particle acceleration.

Understanding the physical mechanisms of turbulent energy dissipation and plasma heating is a fundamental challenge in plasma turbulence research. One type of dissipation mechanism is caused by the resonant wave–particle interactions, such as Landau resonance and cyclotron resonance (Marsch and Tu, 2001; Sahraoui et al., 2009; Camporeale and Burgess, 2011; He JS et al., 2015; Li Z et al., 2019; Chen et al., 2019; Afshari et al., 2021, 2024; Bowen et al., 2022). Previous studies indicate that in solar wind turbulence, energy is mainly dissipated by electron Landau damping into parallel electron heating (Sahraoui et al., 2009), and ions are primarily heated in the perpendicular direction by cyclotron resonance (Bowen et al., 2022). Building on this, Afshari et al. (2021, 2024) further quantified the rates of ion and electron energization by the field–particle correlation technique, identifying that electron Landau damping and ion cyclotron damping play a dominant role in turbulent energy dissipation in the magnetosheath turbulence and determining the partitioning of turbulent energy between species.

Nonresonant wave–particle interactions have also been identified as effective dissipation mechanisms in turbulent plasma. For example, stochastic ion heating occurs when the amplitude of electromagnetic field fluctuations exceeds a critical value, causing chaotic ion motion (Chandran, 2010; Vech et al., 2017; Yoon and Bellan, 2019; Martinović et al., 2020). Additionally, "viscous" heating, which refers to dissipation via pressure anisotropy and kinetic instabilities, is an important mechanism in turbulence (Arzamasskiy et al., 2023; Bandyopadhyay et al., 2023; Yang Y et al., 2024). These mechanisms demonstrate that in collisionless plasmas, wave–particle interactions can dissipate energy and heat particles effectively through various pathways.

Dissipation can also occur within intermittent coherent structures, such as thin current sheets, magnetic islands, and small-scale vortices (Chasapis et al., 2015; Vörös et al., 2017; Yordanova et al., 2020; Jain et al., 2021; Xu QY et al., 2023; Xie ZK et al., 2024). Such structures are usually associated with strong electric currents. Karimabadi et al. (2013) showed that turbulent energy dissipation

First author: Q. Y. Xu, xuqianyun@email.ncu.edu.cn
Correspondence to: M. Zhou, mzhou@ncu.edu.cn
Received 23 OCT 2025; Accepted 19 JAN 2026.
First Published online 05 FEB 2026.

in high-temperature plasmas is primarily due to parallel electric fields associated with the current sheets, leading to anisotropic electron and ion distributions. Their simulation results further indicated that the heating by the current sheet is several orders of magnitude more efficient than wave damping.

Another complementary perspective on understanding turbulent dissipation focuses on tracing energy flow pathways and quantifying conversions between different energy reservoirs. Two parameters are widely used: the electric work on particles $\boldsymbol{J}\cdot\boldsymbol{E}$ (Chasapis et al., 2018; Phan et al., 2018), which quantifies the release of electromagnetic energy, and the pressure–strain interaction Pi-D (Yang Y et al., 2017, 2022, 2023; Bandyopadhyay et al., 2020), which measures the increase in thermal energy. Recent studies have derived a complete Eulerian fluid decomposition of $\boldsymbol{J}_e\cdot\boldsymbol{E}$ and have demonstrated that the diamagnetic drift term is the dominant contributor to electron energization in magnetic reconnection simulations (TenBarge et al., 2024; Steinvall et al., 2025). Yang Y et al. (2023), assessing how protons and electrons respond to different ingredients of the pressure–strain interaction, found that the gyrotropic contribution for electrons is dominant over the nongyrotropic contribution, whereas for protons, nongyrotropic heating is enhanced and protons tend to gain more heating with increasing β. These parameters provide a complementary perspective to the previously discussed dissipation mechanisms.

Identifying all possible mechanisms and their relative contributions is essential for a full understanding of dissipation physics. However, the complexity of turbulence makes it challenging to determine the exact contribution of the different mechanisms. Our previous study of electron heating in the magnetosheath calculated the electron energization rate by using the guiding-center assumption (Xu QY et al., 2023). In this study, we aim to identify the dominant ion energization mechanisms in turbulence. However, ions have a large gyroradius, which leads to the violation of magnetic moment conservation, and the guiding-center description is less applicable. To address this, we utilize a fluid framework derived from the ion momentum equation. This approach does not require the assumption of magnetic moment conservation, and it retains the physical terms omitted in the guiding-center approximation, such as diamagnetic drifts. Using Magnetospheric Multiscale Mission (MMS) observations in the magnetosheath, we quantify and compare the contributions of different ion energization mechanisms and find the critical role of diamagnetic drift. In combination with a previous analysis of electron heating in the magnetosheath (Xu QY et al., 2023), we show the differences in energization mechanisms of the electrons and ions.

2. Methods

To quantitatively analyze the energization mechanisms of ions in collisionless turbulence, we begin with the ion momentum equation in a collisionless plasma:

$$n_i m_i \frac{\mathrm{d}\boldsymbol{v}_i}{\mathrm{d}t} + \nabla\cdot\boldsymbol{P}_i = n_i q_i\left(\boldsymbol{E} + \boldsymbol{v}_i\times\boldsymbol{B}\right). \qquad (1)$$

Here, n_i is the ion density, m_i is the ion mass, $\boldsymbol{v}_i$ is the ion velocity, $\boldsymbol{P}_i$ is the ion pressure tensor, q_i is the particle charge, $\boldsymbol{E}$ is the electric field, $\boldsymbol{B}$ is the magnetic field, and $\frac{\mathrm{d}}{\mathrm{d}t} = \frac{\partial}{\partial t} + \boldsymbol{v}_i\cdot\nabla$. To compute the drifts, we derive the perpendicular component of the ion current density $\boldsymbol{J}_i = n_i q_i \boldsymbol{v}_i$ by cross-multiplying the momentum equation with the magnetic field vector $\boldsymbol{B}$ as

$$\boldsymbol{J}_{i\perp} = -\frac{(\nabla\cdot\boldsymbol{P}_i)\times\boldsymbol{B}}{B^2} - n_i m_i \frac{\mathrm{d}\boldsymbol{v}_i}{\mathrm{d}t}\times\frac{\boldsymbol{B}}{B^2} + n_i q_i \frac{\boldsymbol{E}\times\boldsymbol{B}}{B^2}. \qquad (2)$$

On the right-hand side, the three terms correspond to plasma drift induced by the pressure gradient force, particle inertia, and the $\boldsymbol{E}\times\boldsymbol{B}$ drift effect, respectively. The ion pressure tensor $\boldsymbol{P}_i$ can be decomposed into gyrotropic and nongyrotropic components (Yang Y et al., 2023):

$$\boldsymbol{P}_i = \boldsymbol{P}_{g,i} + \boldsymbol{P}_{ng,i} = p_{i\perp}\boldsymbol{I} + \left(p_{i\parallel} - p_{i\perp}\right)\boldsymbol{bb} + \boldsymbol{P}_{ng,i}, \qquad (3)$$

where $\boldsymbol{P}_{g,i}$ and $\boldsymbol{P}_{ng,i}$ are the gyrotropic (Chew–Goldberger–Low [CGL] pressure tensor) and nongyrotropic parts of the pressure tensor, $\boldsymbol{I}$ is the identity tensor, $p_{i\perp}$ and $p_{i\parallel}$ are the perpendicular and parallel ion pressures to the local magnetic field, defined as $p_{i\perp} = n_i T_{i\perp}$, and $p_{i\parallel} = n_i T_{i\parallel}$, where $T_{i\perp}$ and $T_{i\parallel}$ are the perpendicular and parallel ion temperatures and $\boldsymbol{B} = \boldsymbol{B}/B$ is the unit vector along the local magnetic field. Following the decomposition of the pressure tensor, Equation (2) can be rewritten as

$$\begin{aligned}\boldsymbol{J}_{i\perp} = &-\frac{\nabla p_{i\perp}\times\boldsymbol{B}}{B^2} - \left(p_{i\parallel} - p_{i\perp}\right)\frac{\boldsymbol{k}_c\times\boldsymbol{B}}{B^2} - \frac{\nabla\cdot\boldsymbol{P}_{ng,i}\times\boldsymbol{B}}{B^2} \\ &- n_i m_i \frac{\mathrm{d}\boldsymbol{v}_i}{\mathrm{d}t}\times\frac{\boldsymbol{B}}{B^2} + n_i q_i \frac{\boldsymbol{E}\times\boldsymbol{B}}{B^2},\end{aligned} \qquad (4)$$

where $\boldsymbol{k}_c = (\boldsymbol{B}\cdot\nabla)\boldsymbol{B}$ is the curvature of the magnetic field. The total ion energy gain $\boldsymbol{J}_i\cdot\boldsymbol{E}$ is evaluated by taking the dot of J and E, yielding

$$\begin{aligned}\boldsymbol{J}_i\cdot\boldsymbol{E} = &J_{i\parallel}E_\parallel + \nabla p_{i\perp}\cdot\boldsymbol{v}_E + \left(p_{i\parallel} - p_{i\perp}\right)\boldsymbol{k}_c\cdot\boldsymbol{v}_E + \nabla\cdot\boldsymbol{P}_{ng,i}\cdot\boldsymbol{v}_E \\ &+ n_i m_i \frac{\mathrm{d}\boldsymbol{v}_i}{\mathrm{d}t}\cdot\boldsymbol{v}_E = W_\parallel + W_{\text{diag}} + W_{\text{ani}} + W_{\text{ng}} + W_{\text{in}},\end{aligned} \qquad (5)$$

where $J_{i\parallel}$ is the parallel component of the ion current density, defined as $J_{i\parallel} = q_i n_i v_{i\parallel}$, $E_\parallel$ is the parallel component of the electric field, and $\boldsymbol{v}_E = \boldsymbol{E}\times\boldsymbol{B}/B^2$ is the $\boldsymbol{E}\times\boldsymbol{B}$ drift velocity. On the basis of this decomposition, the total ion energy gain is ultimately expressed as the sum of five independent terms. The first term on the right-hand side of Equation (5) is the direct ion energization by the parallel electric field. The second term is related to the diamagnetic drift. The third term is pressure anisotropy and magnetic field curvature, which work together to drive ion energization, related to the Eulerian curvature drift. The fourth term is due to the nongyrotropic part of the pressure tensor. The last term represents inertial effects. This energization decomposition methodology builds on the framework of fluid compressional and shear mechanisms established by Li XC et al. (2018), combined with the Eulerian and Lagrangian perspective analysis developed by TenBarge et al. (2024). This method is derived from the fluid framework and can accurately describe $\boldsymbol{J}_i\cdot\boldsymbol{E}$. Here, energization denotes the total energy transfer from electromagnetic fields to ions, encompassing both heating (an increase in thermal energy) and acceleration (a change in bulk kinetic energy).

Here, we use the burst mode data from the MMS mission. The magnetic field data were available from the Fluxgate Magnetometer (FGM) instrument (Russell et al., 2016), the electric field data were from the Electric Field Double Probe (EDP) instrument (Ergun et al., 2016), and the ion moments were from the Fast Plasma Investigation (FPI) instrument (Pollock et al., 2016). To ensure temporal alignment of all variables for subsequent calculations, the electromagnetic field data, which have a higher temporal resolution, were interpolated and averaged to 0.15 s to match the time stamps of the ion data. The well-designed tetrahedral formation of the four spacecraft enables an accurate determination of spatial gradients, curvature, and divergence (Paschmann and Daly, 2000). Other parameters (e.g., electromagnetic field, ion density, velocity, temperature) are computed primarily based on the average values from the four MMS spacecraft.

Furthermore, to eliminate the influence caused by the high-speed flow background of the magnetosheath, calculation of the aforementioned five energization terms is performed in a reference frame moving with the magnetosheath flow. Consequently, the ion velocity and electric field transform as $\boldsymbol{v}_i' = \boldsymbol{v}_i - \langle\boldsymbol{v}_i\rangle$, $\boldsymbol{E}' = \boldsymbol{E} + \langle\boldsymbol{v}_i\rangle \times \boldsymbol{B}$, where $\langle\boldsymbol{v}_i\rangle$ represents the average ion bulk velocity over the entire interval.

3. Results

3.1 Case Study

Figure 1 provides an overview of the MMS spacecraft observations from 04:38:03 to 04:46:03 universal time (UT) on November 3, 2018. During this interval, the spacecraft was in the magnetosheath, as seen by the broad energy distribution of ion differential energy flux (Figure 1a) and the high ion density (Figure 1c). The MMS spacecraft was at [−0.2, 23.3, 7.0] R_E (Earth radius) in Geocentric Solar Ecliptic (GSE) coordinates. The tetrahedron quality factor (TQF), defined as the ratio of the actual tetrahedron volume to the volume of a regular tetrahedron with the same interspacecraft distances, is ~0.95. This result indicates that the four satellites form a nearly perfect tetrahedron, allowing a reliable estimation of the gradient of the measured quantities by the MMS by using the multiple spacecraft technique (Paschmann and Daly, 2000; Fuselier et al., 2016).

As shown in Figures 1b and 1d, the magnetic field and plasma flows are highly turbulent, with magnetic field fluctuations reaching $\delta B/\langle B\rangle \sim 0.8$. During this period, the average plasma flow velocity is ~273 km/s (Figure 1d). The average separation between the satellites in the MMS tetrahedron scale is ~15 km, corresponding to ~19 d_e and ~0.4 d_i, where $d_e = c/\omega_{pe}$ and $d_i = c/\omega_{pi}$ represent the electron and ion inertial length, given the average plasma density of ~42 cm^{-3}.

Figures 1f–1j detail the power densities of the five individual ion energization terms: the parallel electric field acceleration $W_{||}$, the diamagnetic drift term $W_{\rm diag}$, the anisotropy term $W_{\rm ani}$, the nongyrotropic term $W_{\rm ng}$, and the inertial drift term $W_{\rm in}$. The calculations are based on multipoint measurements of the electromagnetic fields and ion moments from the four spacecraft. Figures 1f–1j show the presence of both positive and negative energization rates, suggesting a bidirectional energy exchange between electromagnetic fields and ions. The terms $W_{\rm diag}$, $W_{\rm ng}$, and $W_{\rm in}$ exhibit greater fluctuations compared with $W_{||}$ and $W_{\rm ani}$.

To compare the effects of different ion energization terms, we examine the probability distribution functions (PDFs) of the power densities in Figure 2. The distribution of $W_{\rm diag}$ (blue line) shows the widest spread and positive skewness, indicating that $W_{\rm diag}$ generally exceeds the other four energization terms. The average values for $W_{||}$, $W_{\rm ani}$, $W_{\rm diag}$, $W_{\rm ng}$, and $W_{\rm in}$ are −2, −1, 62, −15, and −5 eV·s^{-1}·cm^{-3}, respectively, with the total ion energization $W_{\rm sum}$ (sum of the five distinct ion energization terms) averaging 42 eV·s^{-1}·cm^{-3}. This result suggests that $W_{\rm diag}$ is the dominant contributor to ion energization during this event, whereas the other four mechanisms, on average, result in ion energy loss during this event.

The spatial scale of the magnetic field (L_{dB}) has been proposed to delineate the scale at which acceleration occurs (Xu QY et al., 2023). The L_{dB} is calculated using multiple spacecraft measurements. It assumes linear spatial variation within the MMS tetrahedron (Chanteur, 1998). As defined in Equation (6), the spatial scale of the magnetic field is

$$L_{dB} = B/|\nabla\boldsymbol{B}|, \tag{6}$$

where $|\nabla\boldsymbol{B}|$ is the norm of the Jacobian matrix of the magnetic field, expressed as $|\nabla\boldsymbol{B}| = \sqrt{\sum_{ij}\left(\frac{\partial B_i}{\partial x_j}\right)^2}$ (Kress et al., 2007).

Figure 3a shows how the $W_{\rm sum}$ changes with the spatial scale L_{dB}. The $W_{\rm sum}$ exhibits a U-shaped relationship with L_{dB}—initially decreasing as the scale increases, stabilizing at intermediate scales, and finally showing a slight enhancement at the largest scales. Ion energization mainly occurs at scales below the ion inertial scale, where the turbulent energy cascade is expected to dissipate at kinetic scales. Figure 3b further illustrates the variations of the five individual ion energization terms as a function of L_{dB}. As shown in Figure 3b, $W_{\rm diag}$ is mostly positive and stronger than the other four terms across most scales, being the main ion energization source. However, at large scales ($L > 37\ d_i$), the contributions from $W_{\rm in}$ and $W_{\rm ng}$ rise to levels comparable with those of $W_{\rm diag}$.

We further utilized the partial variance of increments (PVI) method to examine the relationship between ion energization and the coherent structures. The PVI method was developed for detecting coherent structures in turbulence (Chasapis et al., 2015; Vörös et al., 2017; Yordanova et al., 2020; Xu QY et al., 2023). The PVI index can be estimated as follows:

$$\mathrm{PVI}_{ij}(t) = \sqrt{\frac{|\boldsymbol{B}_i(t) - \boldsymbol{B}_j(t)|^2}{\left\langle|\boldsymbol{B}_i(t) - \boldsymbol{B}_j(t)|^2\right\rangle}}, \tag{7}$$

where the subscript i, j = 1, 2, 3, 4 indicates the different MMS spacecraft.

Figure 3c shows the ion energization conditioned on the PVI index. As shown in Figure 3c, the average $W_{\rm sum}$ exhibits an overall positive correlation with the PVI index, except for a slight decrease near PVI ~1.5. This indicates that a larger PVI corresponds to stronger ion energization. Among the five ion energization terms, $W_{\rm diag}$ also shows a trend of increasing with an increase in the PVI index. In contrast, the other four parameters remain near zero, with little variation. This finding confirms that the enhancement

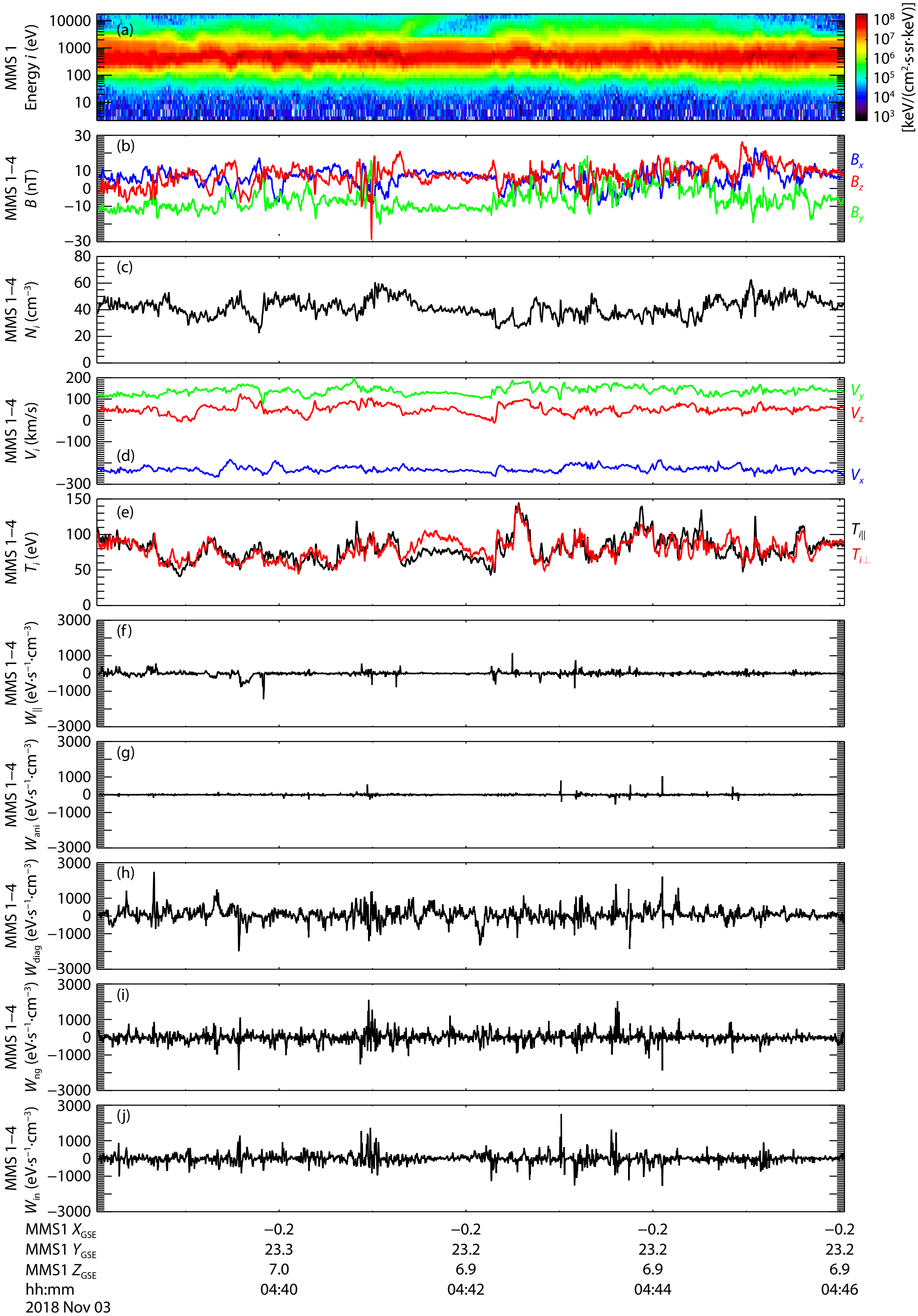

Figure 1. Overview of the turbulence in the magnetosheath observed by the MMS from 04:38:03 to 04:46:03 universal time (UT) on November 3, 2018. Top to bottom: (a) ion differential energy flux by MMS1; (b–e) four spacecraft averages of (b) three components of the magnetic field and (c) the ion density; (d) three components of the ion bulk velocity; (e) ion parallel and perpendicular temperatures; (f–j) the ion energization terms appearing in Equation (5): $W_{\|}$, W_{ani}, W_{diag}, W_{ng}, W_{in}, respectively. The vectors are displayed in the Geocentric Solar Ecliptic (GSE) coordinate system.

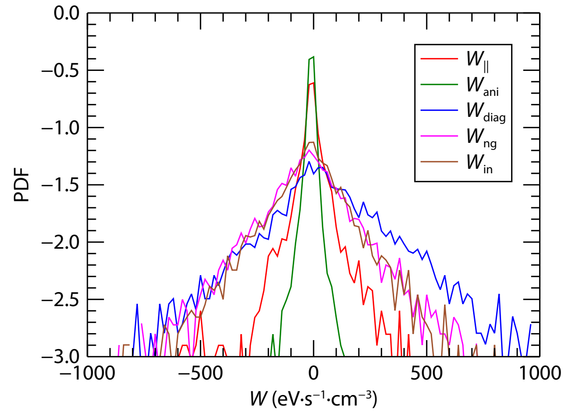

Figure 2. The probability distribution function (PDF) of ion energization terms, $W_{||}$ (red), W_{ani} (green), W_{diag} (blue), W_{ng} (pink), and W_{in} (brown).

of W_{sum} is primarily contributed by W_{diag}, with negligible contributions from the other terms. We also notice that the ion temperature is positively correlated with the PVI index (Figure 3d), suggesting that the coherent structures with a large PVI index contribute to ion energization and heating.

3.2 Statistical Analysis

To investigate statistical behavior, 35 intervals of MMS burst data observed in Earth's magnetosheath between October 2015 and February 2020 were selected (Table 1 details these intervals). These intervals were drawn from published magnetosheath turbulence databases (Wang YW et al., 2021; Stawarz et al., 2022; Yang Y et al., 2023; Lewis et al., 2024) and filtered to retain those longer than 5 min with a tetrahedron quality factor (TQF) greater than 0.6. Although turbulent energy transfer is bidirectional, this study focuses on net ion energization ($\langle W_{sum}\rangle > 0$). Of the 75 intervals meeting the initial criteria, 35 intervals satisfy this condition.

For each interval, we calculate the average ion energization $\langle W_i\rangle$ over the whole interval, as shown in Table 1. To compare the relative contribution of different ion energization mechanisms, these averaged values were normalized as $\langle W_i\rangle / \sum|\langle W_j\rangle|$, where $i, j = ||$, ani, diag, ng, in. This normalization ratio retains the sign information of energization terms while transforming ion energization values into dimensionless relative contributions.

The statistical distribution of these values for net ion energization events is shown in Figure 4. The unnormalized $<W_{sum}>$ is displayed in Figure 4a. We see that it is distributed between 0

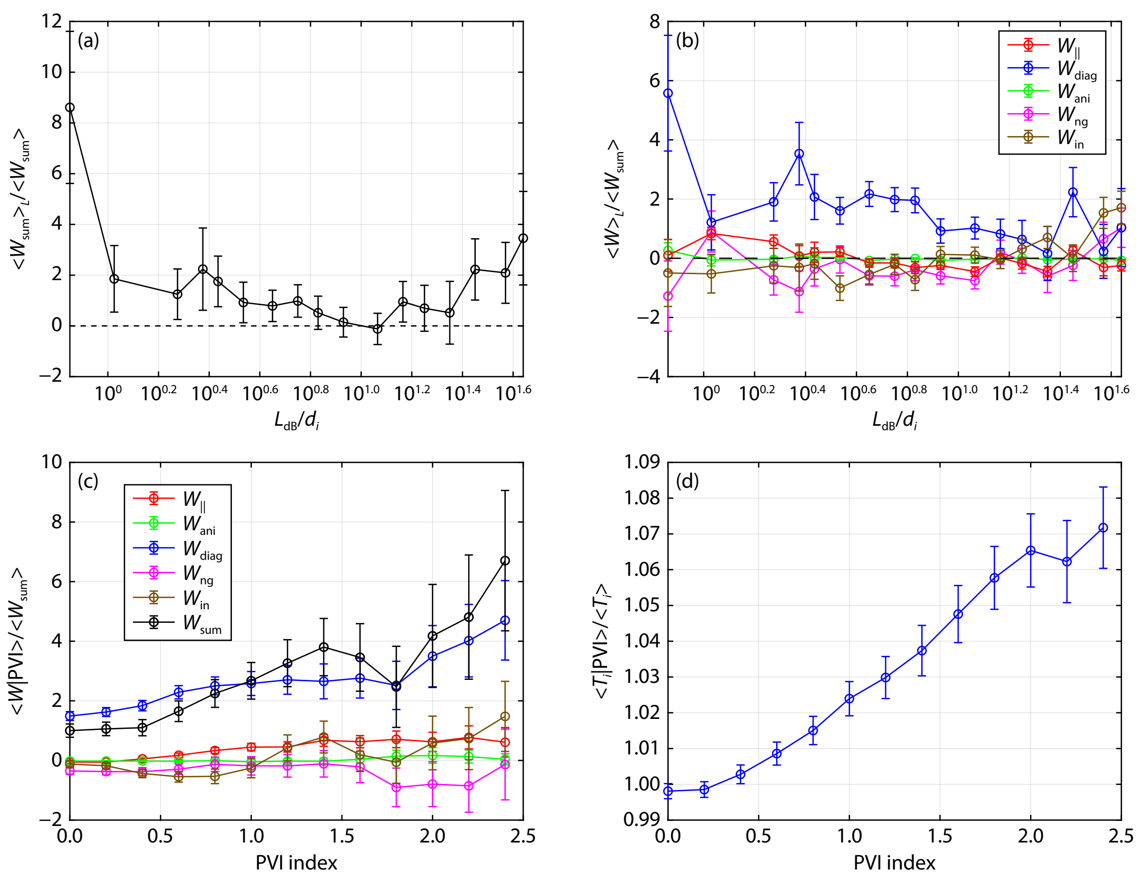

Figure 3. (a) The average of total ion energization $<W_{sum}>_L/<W_{sum}>$ and (b) each ion energization term W_j ($j = ||$, ani, diag, ng, in) as a function of L_{dB}, where $< >_L$ denotes the bin-averaged value of W over scale L, normalized by $<W_{sum}>$, the global average of W_{sum}. (c) The average of each ion energization term and (d) the ion temperature conditioned on the binned partial variance of increments (PVI) index. The notation $<W|PVI>$ denotes the average of W calculated over all samples where the local PVI value exceeds the value indicated on the horizontal axis. The ion temperature is normalized by $<T_i>$ in a moving window with a duration of 4 s. The vertical bars in the panels represent the standard errors of the mean.

Table 1. The time intervals of net ion energization events in magnetosheath turbulence.[a]

Index	Time range (UTC)	$<\beta_i>$	$<W_{sum}>$	$<W_{\|\|}>$	$<W_{ani}>$	$<W_{diag}>$	$<W_{ng}>$	$<W_{in}>$
1	2015-10-21/06:55:10–07:03:45	5.7	362	4	31	410	66	−142
2	2015-10-29/14:48:05–14:53:55	1.8	15	4	−1	24	−3	−8
3	2016-12-09/09:26:25–09:34:57	4.7	668	−132	−9	350	−231	692
4	2016-12-18/07:08:34–07:18:14	4.8	46	−25	11	135	51	−129
5	2017-01-27/00:52:47–01:02:36	5.5	539	−4	−51	522	533	−500
6	2017-01-27/08:02:03–08:08:03	8.0	481	−94	−19	21	587	−3
7	2017-01-28/09:05:25–09:11:12	9.0	168	−24	18	20	98	57
8	2017-11-16/15:36:06–15:44:09	6.4	114	48	8	125	7	−67
9	2017-12-06/11:06:03–11:12:43	4.6	50	−1	2	59	3	−13
10	2017-12-09/06:12:33–06:18:22	6.7	26	−8	0.1	76	−12	−26
11	2017-12-21/06:41:50–07:03:51	8.0	7	4	4	−0.3	11	−12
12	2017-12-26/05:46:16–06:03:00	5.2	49	−15	0.001	73	−4	−5
13	2017-12-26/06:12:43–06:52:23	4.1	13	−19	−3	48	−10	−5
14	2018-01-21/06:50:53–06:56:33	6.5	695	73	−1	240	281	103
15	2018-02-10/00:55:03–01:00:34	20.0	16	−1	−26	55	40	−51
16	2018-02-18/12:52:43–13:03:02	5.1	73	2	−1	110	−21	−15
17	2018-03-01/20:19:23–20:27:43	14.5	26	−6	1	31	4	−3
18	2018-03-15/21:25:43–21:32:53	4.9	48	−2	1	67	−5	−12
19	2018-04-14/23:00:13–23:06:15	4.6	9	1	−2	35	7	−29
20	2018-04-23/07:50:12–08:33:41	6.3	14	−4	1	28	6	−16
21	2018-04-27/17:56:24–18:03:50	8.0	71	16	13	31	32	−16
22	2018-04-28/21:29:05–21:34:21	7.4	0.4	0.1	−0.2	2	1	−2
23	2018-05-23/14:35:25–14:41:42	9.9	21	11	0.2	−2	4	8
24	2018-05-28/22:23:39–22:30:31	1.0	1	−0.1	−0.05	5	1	−4
25	2018-10-27/09:13:14–09:57:41	13.5	31	5	−1	17	15	−5
26	2018-11-03/04:38:03–04:46:03	6.1	42	−2	−1	62	−15	−5
27	2018-11-29/22:42:34–23:31:01	9.4	38	23	10	9	25	−28
28	2018-12-05/14:53:23–15:20:13	7.1	47	47	30	−5	24	−48
29	2018-12-18/20:02:03–20:16:01	8.3	63	2	17	74	−2	−27
30	2018-12-18/20:36:03–20:45:21	11.0	49	2	3	41	18	−14
31	2018-12-22/13:12:03–13:22:53	6.2	15	40	−5	−22	4	−5
32	2019-10-09/07:12:14–07:18:00	7.4	14	0.3	0.2	15	−3	2
33	2019-10-10/09:02:44–09:10:00	14.7	75	3	3	41	32	5
34	2019-12-24/01:33:04–01:46:11	16.1	2	6	1	−7	−2	3
35	2020-02-26/00:23:54–01:20:00	5.9	54	42	2	17	9	−17

[a]The table lists the average ion beta and the mean values of the ion energization terms, with units of electron volts per second per cubic centimeter.

and 700 $eV \cdot s^{-1} \cdot cm^{-3}$ and predominantly concentrated within 100 $eV \cdot s^{-1} \cdot cm^{-3}$. Figures 4b–4f show that the W_{diag} exhibits a significantly positive and dominant contribution ratio, whereas the other four terms predominantly cluster near zero. The bias in statistical distributions, such as $W_{||}$, W_{in}, and W_{ng}, is a positive bias, whereas W_{ani} exhibits a negative bias. This reflects their respective ion energization enhancements or suppression effects, although weaker than W_{diag}. The largest and positive $<W_i>$ in each interval is considered the dominant term. The statistical results of 35 intervals show that diamagnetic drift (W_{diag}) serves as the predominant ion energization mechanism, accounting for 62.9% of all the examined events (22 intervals). The contributions of other terms are less: nongyrotropic pressure (W_{ng}), the parallel electric field ($W_{||}$), and inertial effects (W_{in}) dominate 7 (20%), 5 (14.3%), and 1 (2.8%) intervals, respectively.

To present a complete picture of turbulent energy transfer, we extend our analysis to intervals exhibiting net ion energy loss

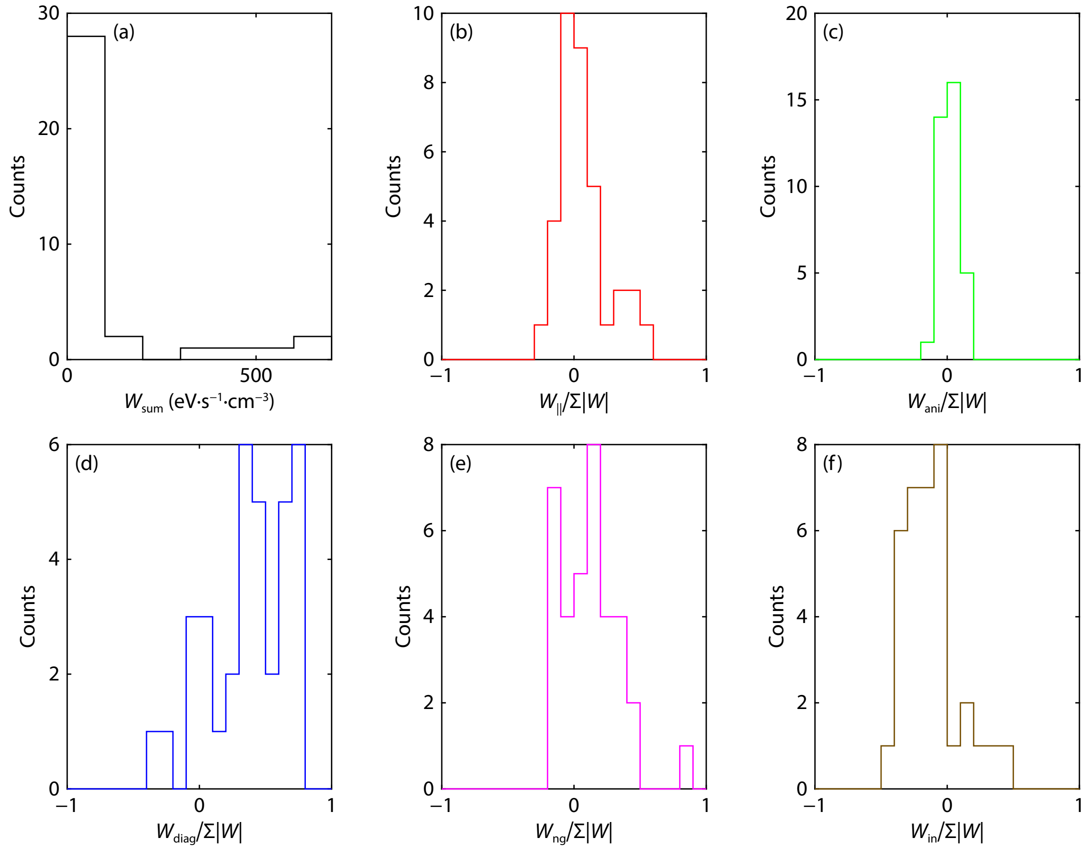

Figure 4. Statistical results of 35 net ion energization intervals in magnetosheath turbulence. (a) Histogram distribution of $\langle W_{sum}\rangle$, where $\langle\cdots\rangle$ means the average of each whole interval. The vertical axis indicates the frequency of event occurrences. (b–f) Histogram distribution of ion energization terms. The horizontal axis shows the normalized relative contribution of ion energization ($\langle W_i\rangle / \sum|\langle W\rangle|$, where i = ||, ani, diag, ng, in), $\sum W$ represents the sum of the absolute values of all energization terms.

($\langle W_{sum}\rangle < 0$). The corresponding statistical distribution for these 40 net energy loss intervals is provided in the Supplementary Materials (Figure S1). A key finding is that the diamagnetic drift (W_{diag}) remains the dominant mechanism not only for energy gain but also for energy loss, confirming its role as a primary and reversible energy channel in the turbulence.

By aggregating data from all 35 intervals, we statistically studied the scale dependence of ion energization by a similar method. As shown in Figure 5a, W_{sum} is predominantly concentrated at small scales (~0.2 d_i) and descends with an increment of the spatial scale. The characteristics are similar to those of electrons but occur on a wider scale (~$10^{1.5}$ d_i). Notably, the ion energization exhibits significant uncertainties at scales $L < 10^{-0.8}$ d_i, which are consequently ignored in our analysis.

However, no clear relationship is observed between ion energization/heating and coherent structures, as is found in electrons. Figures 5b and 5c present the variation in ion energization and ion temperature with the PVI index, each line representing an interval. We see positive correlations, negative correlations, and weak correlations, with no unified conclusion.

4. Discussion and Conclusions

Previous studies have shown that energy dissipation and ion heat-

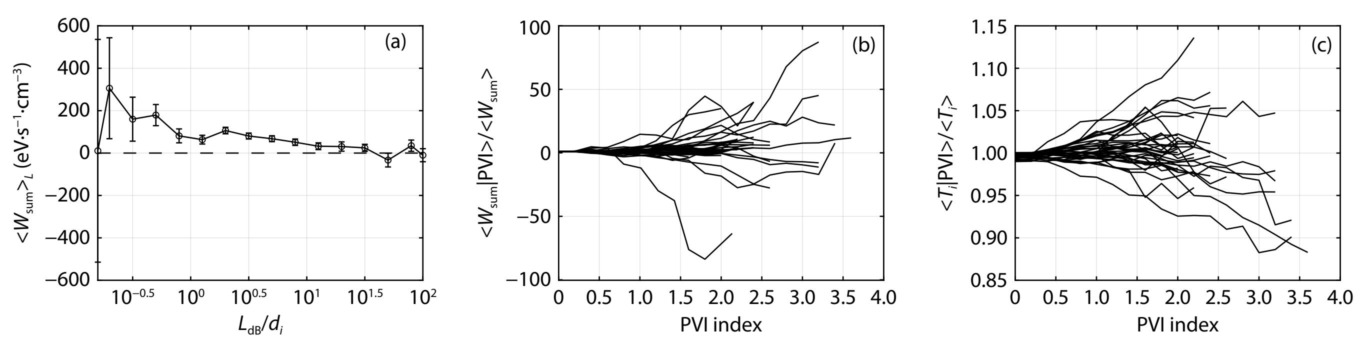

Figure 5. (a) The average $<W_{sum}>$ as a function of L_{dB}, sampled by MMS, corresponding to the 35 intervals. (b, c) The total ion energization W_{sum} and the ion temperature conditioned on the binned PVI index, each line representing an interval.

ing in turbulence may occur through processes such as Landau resonance, cyclotron resonance, and stochastic ion heating (He JS et al., 2015; Vech et al., 2017; Yoon and Bellan, 2019; Bowen et al., 2022; Afshari et al., 2024). Landau damping is linked to parallel electric field acceleration; however, our results indicate that $W_{||}$ is not the dominant mechanism for ion energization. Wave–particle interaction through cyclotron resonance typically results in temporal variation of the bulk velocity and the electric field, which essentially corresponds to the energization quantified by W_{in}. Here, we see that W_{in} is often negative, causing ions to lose energy. In addition, the cyclotron resonance is closely connected to the temperature anisotropy, corresponding to W_{ani}, which is always smaller than the other terms. Stochastic ion heating occurs when electromagnetic field fluctuations exceed a critical level at the ion cyclotron scale, making ion motion chaotic and causing perpendicular heating, corresponding to W_{ng}. We found that this term plays a role in ion energization but is not the dominant one.

In contrast, our study finds that diamagnetic drift is the dominant ion energization mechanism, contributing to 62.9% of the net ion energization events. This finding provides a crucial new perspective on ion energy gain. Although W_{diag} dominates the energization, diamagnetic drift itself is not a direct heating mechanism but represents the work done via the $E \times B$ drift acting on ion pressure gradients. This is a macroscopic, fluid-scale energy conversion process that includes the energy fluxes and fluid drifts whose dominance does not rely on rapid microscopic particle responses. Consequently, even though individual ions have a large mass and respond slowly, the ion fluid can efficiently extract energy through this channel.

Furthermore, the electric field used in this study, measured directly by the MMS, is a composite field encompassing multiple physical processes. We may infer the origin of the electric field through the ion momentum equation. Because the W_{diag} term is the dominant term in ion energization, the ion pressure gradient term is significantly larger than the ion inertial term in the ion momentum equation. The ion convection electric field $-V_i \times B$ is generally the first-order term; thus, the electric field in the turbulent magnetosheath is probably contributed mainly by the motional electric field from ion bulk flow and the divergence of the ion pressure tensor.

Crucially, W_{diag} dominates both ion gain energization and loss energization. This symmetry confirms its role as a primary and reversible energy channel in turbulence, facilitating efficient bidirectional energy exchange between the electromagnetic fields and ions.

A further question is the difference in the energy gain between ions and electrons. We find that the main energy transport channels for electrons and ions are different. Afshari et al. (2021) found that 95% of the intervals have velocity–space signatures of electron Landau damping in the magnetosheath. Xu QY et al. (2023) reported that electrons are primarily accelerated by the parallel electric field around the ion inertial length within coherent structures. However, this study shows that ions mainly gain energy through diamagnetic drift and that parallel electric field acceleration $W_{||}$ dominates in only 14% of intervals. Another difference is that ion energization occurs on a larger scale than electron acceleration. The case study shows that ion energization occurs not only at small scales but also at large scales, where it is enhanced by inertial effects (W_{in}) and nongyrotropic pressure (W_{ng}) processes. Statistical results show that ion energization is mainly concentrated at small scales and descends with an increment of the spatial scale. This is similar to the previously reported scale characteristics of electron acceleration, but ion energization occurs on a wider scale than electrons, extending up to approximately 30 d_i (Xu QY et al., 2023).

Although both ion energization and ion temperature are strongly positively correlated with PVI in the representative cases, the statistical analysis shows more possibilities. On one hand, coherent structures often maintain internally organized correlations and can therefore be less sensitive to background fluctuations (Yao ST et al., 2017; Shi QQ et al., 2024). On the other hand, such structures may also be influenced by turbulence through complex interactions (Yao ST et al., 2020). Therefore, from a holistic statistical perspective, the relationship manifests as considerable uncertainty.

This result might be due to different background conditions, such as amplitude of turbulent fluctuations, plasma β, and so forth. Additionally, structures such as magnetic holes, mirror modes, and current sheets typically occur in weakly magnetized environments where the magnetic moment is not conserved (Liu J et al., 2020, Yao ST et al., 2021). Thus, differences in magnetization state may also influence the behavior of energization mechanisms, representing a potential direction for future research. The results suggest the complexity and diversity of energy dissipation and particle acceleration in turbulence, offering a richer perspective on understanding space plasma heating.

In summary, this study systematically quantifies the effects of different mechanisms on ion energization in magnetosheath turbulence by using MMS observations. We find that diamagnetic drift is the dominant mechanism for ion energization and that it occurs mainly around the ion inertial length, but on a larger scale than electrons. The relationship between ion energization/heating and coherent structures remains unclear and requires further research. This study provides key observational evidence to advance the understanding of turbulent energy dissipation and particle heating mechanisms.

Acknowledgments

We thank the MMS team for providing the high-quality data to complete this work. This work was supported by the National Natural Science Foundation of China (NSFC) under Grant Numbers 42074197, 42130211, and 41774154.

Data Availability Statement

The data used in this study were obtained from the MMS Science Data Center (https://lasp.colorado.edu/mms/sdc/public/about/browse-wrapper/).

Supplementary Materials

To provide a complete picture of turbulent energy transfer, we extend our analysis to intervals where the net ion energization is negative ($<W_{sum}> < 0$). Table S1 lists 40 intervals with net ion energy loss. Figure S1 shows the statistical distribution of net ion energy loss intervals. Diamagnetic drift (W_{diag}) and inertial effects (W_{in}) are the primary mechanisms for ion energy loss, each dominating in 18 out of the 40 intervals (45% each). This finding is pivotal: W_{diag} is the dominant mechanism for energy gain; it is also the most prevalent mechanism for energy loss. It confirms that

Table S1. The time intervals of net ion energy loss events in magnetosheath turbulence. The units are the same as in Table 1.

Index	Time range (UTC)	$<\beta_i>$	$<W_{sum}>$	$<W_{\parallel}>$	$<W_{ani}>$	$<W_{diag}>$	$<W_{ng}>$	$<W_{in}>$
1	2016-01-24/23:36:14–23:47:34	9.8	−142	−26	−1	82	16	−48
2	2016-09-28/16:00:00–16:08:52	1.3	−15	−5	1	−10	6	−10
3	2016-09-28/16:50:14–17:00:14	2.0	−283	−7	−11	−256	43	−51
4	2016-09-30/17:50:34–18:01:50	1.2	−53	−5	−0.5	−137	115	−39
5	2016-10-01/18:30:00–18:40:00	1.6	−348	3	1	−349	46	−50
6	2016-12-09/09:01:40–09:07:00	5.2	−300	44	−67	−96	127	−279
7	2016-12-11/15:20:14–15:32:34	10.7	−523	29	0.4	−128	−288	−134
8	2017-01-28/05:29:14–05:34:50	5.4	−966	−62	65	−781	78	−234
9	2017-01-31/04:19:33–04:35:13	42.7	−846	90	92	−690	−288	−82
10	2017-09-28/06:31:33–07:01:43	5.7	−152	−8	0.3	−96	−32	−23
11	2017-09-28/10:43:00–10:53:30	9.9	−31	−18	1	−24	16	−3
12	2017-09-28/20:42:00–20:51:21	7.1	−38	23	−2	−21	9	−46
13	2017-11-10/22:04:43–22:15:33	8.1	−176	−38	−11	−47	−35	−48
14	2017-11-10/22:35:43–22:52:03	7.0	−20	4	9	10	27	−73
15	2017-11-13/19:30:42–19:38:43	6.5	−9	−1	−0.1	−27	33	−13
16	2017-12-01/13:12:07–13:23:38	9.8	−16	−20	−12	44	8	−38
17	2017-12-21/07:21:54–07:48:01	4.4	−10	−5	13	−5	267	−37
18	2018-02-21/07:48:53–08:01:43	6.2	−5	37	13	178	17	−239
19	2018-03-15/20:32:00–20:38:42	2.3	−10	−1	0.5	16	−5	−19
20	2018-04-19/05:08:04–05:41:53	12.5	−10	−7	0.03	3	7	−14
21	2018-04-24/21:44:14–21:52:32	5.2	−58	−20	−3	3	−6	−29
22	2018-04-27/17:35:43–17:41:52	15.2	−194	−27	−4	−155	1	−23
23	2018-04-28/21:02:04–21:09:21	5.8	−14	1	1	−10	3	−10
24	2018-04-28/22:22:45–22:29:41	10.7	−28	2	−1	−39	4	5
25	2018-10-16/14:22:13–14:32:13	13.1	−25	−0.1	2	−28	1	1
26	2018-10-22/07:23:23–07:35:03	7.0	−47	7	−2	−21	4	−34
27	2018-10-28/11:26:33–11:45:23	4.0	−51	9	−7	−16	3	−40
28	2018-11-01/22:16:13–22:31:43	6.8	−45	−0.3	0.1	−20	−6	−19
29	2018-11-07/13:13:03–13:37:33	4.3	−129	41	27	−59	−51	−84
30	2018-11-21/16:10:14–16:55:31	5.1	−9	4	0.1	4	−0.4	−17
31	2018-12-01/23:04:03–23:12:23	10.1	−258	−50	11	−169	−12	−35
32	2019-04-02/21:54:33–22:05:23	4.9	−103	−9	3	3	−6	−91
33	2019-04-05/11:30:53–12:03:12	4.2	−8	42	−3	−37	48	−62
34	2019-10-10/15:00:00–15:07:21	5.6	−21	0.2	2	−17	−7	0.1
35	2019-10-16/12:54:24–13:16:00	11.4	−32	−22	−1	−3	1	−7
36	2019-11-05/22:04:54–22:13:42	7.5	−55	10	−1	−57	−6	−2
37	2019-11-19/21:45:00–21:53:00	12.3	−17	−0.1	−1	−7	−9	−0.03
38	2019-11-25/13:20:00–13:40:00	8.6	−12	−3	−0.3	0.1	−8	−2
39	2019-12-07/09:50:01–10:30:00	7.1	−58	−8	5	−10	−18	−26
40	2019-12-31/23:46:00–23:57:00	3.6	−30	−2	5	−11	−1	−21

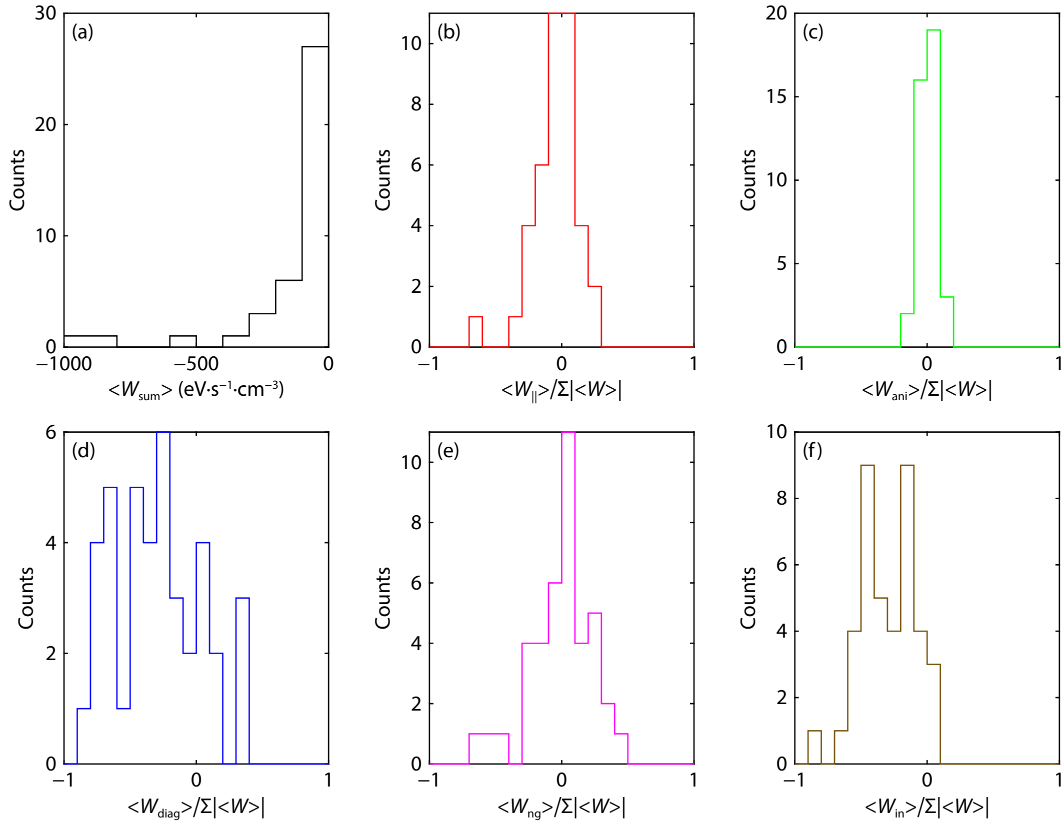

Figure S1. Statistical results of net ion loss energy intervals in magnetosheath turbulence. (a) Histogram distribution of <W_{sum}>. (b–f) Histogram distribution of ion energization terms. The panel arrangement is consistent with that of Figure 4.

W_{diag} is a reversible energy channel in plasma turbulence. Energy is efficiently transferred back and forth through this mechanism. The bias in the statistical distribution of W_{in} is always negative bias for both net ion gain and loss events. The processes with ion inertia consistently facilitate ion loss energy on average, regardless of the overall energy state of the interval.

References

Afshari, A. S., Howes, G. G., Kletzing, C. A., Hartley, D. P., and Boardsen, S. A. (2021). The importance of electron Landau damping for the dissipation of turbulent energy in terrestrial magnetosheath plasma. *J. Geophys. Res.: Space Phys.*, *126*(12), e2021JA029578. https://doi.org/10.1029/2021JA029578

Afshari, A. S., Howes, G. G., Shuster, J. R., Klein, K. G., McGinnis, D., Martinović, M. M., Boardsen, S. A., Brown, C. R., Huang, R., … Kletzing, C. A. (2024). Direct observation of ion cyclotron damping of turbulence in Earth's magnetosheath plasma. *Nat. Commun.*, *15*(1), 7870. https://doi.org/10.1038/s41467-024-52125-8

Arzamasskiy, L., Kunz, M. W., Squire, J., Quataert, E., and Schekochihin, A. A. (2023). Kinetic turbulence in collisionless high-β plasmas. *Phys. Rev. X*, *13*(2), 021014. https://doi.org/10.1103/PhysRevX.13.021014

Bandyopadhyay, R., Matthaeus, W. H., Parashar, T. N., Yang, Y., Chasapis, A., Giles, B. L., Gershman, D. J., Pollock, C. J., Russell, C. T., … Burch, J. L. (2020). Statistics of kinetic dissipation in the Earth's magnetosheath: MMS observations. *Phys. Rev. Lett.*, *124*(25), 255101. https://doi.org/10.1103/PhysRevLett.124.255101

Bandyopadhyay, R., Yang, Y., Matthaeus, W. H., Parashar, T. N., Roytershteyn, V., Chasapis, A., Gershman, D. J., Giles, B. L., and Burch, J. L. (2023). Collisional-like dissipation in collisionless plasmas. *Phys. Plasmas*, *30*(8), 080702. https://doi.org/10.1063/5.0146986

Bowen, T. A., Chandran, B. D. G., Squire, J., Bale, S. D., Duan, D., Klein, K. G., Larson, D., Mallet, A., McManus, M. D., … Woodham, L. D. (2022). *In situ* signature of cyclotron resonant heating in the solar wind. *Phys. Rev. Lett.*, *129*(16), 165101. https://doi.org/10.1103/PhysRevLett.129.165101

Camporeale, E., and Burgess, D. (2011). The dissipation of solar wind turbulent fluctuations at electron scales. *Astrophys. J.*, *730*(2), 114. https://doi.org/10.1088/0004-637X/730/2/114

Chandran, B. D. G. (2010). Alfvén-wave turbulence and perpendicular ion temperatures in coronal holes. *Astrophys. J.*, *720*(1), 548–554. https://doi.org/10.1088/0004-637X/720/1/548

Chanteur, G. (1998). Spatial Interpolation for Four Spacecraft: Theory. In G. Paschmann and P. W. Daly (Eds.), *Analysis Methods for Multi-Spacecraft Data* (pp. 349–369). Noordwijk, The Netherlands: ESA Publications Division.

Chasapis, A., Retinò, A., Sahraoui, F., Vaivads, A., Khotyaintsev, Y. V., Sundkvist, D., Greco, A., Sorriso-Valvo, L., and Canu, P. (2015). Thin current sheets and associated electron heating in turbulent space plasma. *Astrophys. J.*, *804*(1), L1. https://doi.org/10.1088/2041-8205/804/1/L1

Chasapis, A., Matthaeus, W. H., Parashar, T. N., Wan, M., Haggerty, C. C., Pollock, C. J., Giles, B. L., Paterson, W. R., Dorelli, J., … Burch, J. L. (2018). In situ observation of intermittent dissipation at kinetic scales in the Earth's magnetosheath. *Astrophys. J.*, *856*(1), L19. https://doi.org/10.3847/2041-8213/aaadf8

Chen, C. H. K., Klein, K. G., and Howes, G. G. (2019). Evidence for electron Landau damping in space plasma turbulence. *Nat. Commun.*, *10*(1), 740. https://doi.org/10.1038/s41467-019-08435-3

Ergun, R. E., Tucker, S., Westfall, J., Goodrich, K. A., Malaspina, D. M., Summers, D., Wallace, J., Karlsson, M., Mack, J., … Cully, C. M. (2016). The axial double probe and fields signal processing for the MMS mission. *Space Sci. Rev.*, *199*(1–4), 167–188. https://doi.org/10.1007/s11214-014-0115-x

Fuselier, S. A., Lewis, W. S., Schiff, C., Ergun, R., Burch, J. L., Petrinec, S. M., and Trattner, K. J. (2016). Magnetospheric multiscale science mission profile and operations. *Space Sci. Rev.*, *199*(1–4), 77–103. https://doi.org/10.1007/s11214-014-0087-x

He, J. S., Wang, L. H., Tu, C. Y., Marsch, E., and Zong, Q. G. (2015). Evidence of Landau and cyclotron resonance between protons and kinetic waves in solar wind turbulence. *Astrophys. J.*, *800*(2), L31. https://doi.org/10.1088/2041-8205/800/2/L31

Jain, N., Büchner, J., Comişel, H., and Motschmann, U. (2021). Free energy sources in current sheets formed in collisionless plasma turbulence. *Astrophys. J.*, *919*(2), 103. https://doi.org/10.3847/1538-4357/ac106c

Karimabadi, H., Roytershteyn, V., Wan, M., Matthaeus, W. H., Daughton, W., Wu, P., Shay, M., Loring, B., Borovsky, J., … Nakamura, T. K. M. (2013). Coherent structures, intermittent turbulence, and dissipation in high-temperature plasmas. *Phys. Plasmas*, *20*(1), 012303. https://doi.org/10.1063/1.4773205

Kress, B. T., Hudson, M. K., Looper, M. D., Albert, J., Lyon, J. G., and Goodrich, C. C. (2007). Global MHD test particle simulations of >10 MeV radiation belt electrons during storm sudden commencement. *J. Geophys. Res.: Space Phys.*, *112*(A9), A09215. https://doi.org/10.1029/2006JA012218

Lewis, H. C., Stawarz, J. E., Matteini, L., Franci, L., Klein, K. G., Wicks, R. T., Salem, C. S., Horbury, T. S., and Wang, J. H. (2024). Turbulent energy conversion associated with kinetic microinstabilities in Earth's magnetosheath. *Geophys. Res. Lett.*, *51*(24), e2024GL112038. https://doi.org/10.1029/2024GL112038

Li, X. C., Guo, F., Li, H., and Birn, J. (2018). The roles of fluid compression and shear in electron energization during magnetic reconnection. *Astrophys. J.*, *855*(2), 80. https://doi.org/10.3847/1538-4357/aaacd5

Li, Z., Lu, Q., Wang, R., Gao, X., Chen, H. (2019). In situ evidence of resonant interactions between energetic electrons and whistler waves in magnetopause reconnection. *Earth Planet. Phys.*, *3*(6), 1–7. https://doi.org/10.26464/epp2019048

Liu, J., Yao, S. T., Shi, Q. Q., Wang, X. G., Zong, Q. G., Feng, Y. Y., Liu, H., Guo, R. L., Yao, Z. H., … Giles, B. L. (2020). Electron energization and energy dissipation in microscale electromagnetic environments. *Astrophys. J. Lett.*, *899*(2), L31. https://doi.org/10.3847/2041-8213/abab92

Marsch, E., and Tu, C. Y. (2001). Heating and acceleration of coronal ions interacting with plasma waves through cyclotron and Landau resonance. *J. Geophys. Res.: Space Phys.*, *106*(A1), 227–238. https://doi.org/10.1029/2000JA000042

Martinović, M. M., Klein, K. G., Kasper, J. C., Case, A. W., Korreck, K. E., Larson, D., Livi, R., Stevens, M., Whittlesey, P., … MacDowall, R. J. (2020). The enhancement of proton stochastic heating in the near-sun solar wind. *The Astrophysical Journal Supplement Series*, *246*(2), 30. https://doi.org/10.3847/1538-4365/ab527f

Paschmann, G., and Daly, P. W. (2000). *Analysis Methods for Multi-Spacecraft Data*. Noordwijk, The Netherlands: ESA Publications Division.

Phan, T. D., Eastwood, J. P., Shay, M. A., Drake, J. F., Sonnerup, B. U. Ö., Fujimoto, M., Cassak, P. A., Øieroset, M., Burch, J. L., … Magnes, W. (2018). Electron magnetic reconnection without ion coupling in Earth's turbulent magnetosheath. *Nature*, *557*(7704), 202–206. https://doi.org/10.1038/s41586-018-0091-5

Pollock, C., Moore, T., Jacques, A., Burch, J., Gliese, U., Saito, Y., Omoto, T., Avanov, L., Barrie, A., … Zeuch, M. (2016). Fast plasma investigation for magnetospheric multiscale. *Space Sci. Rev.*, *199*(1–4), 331–406. https://doi.org/10.1007/s11214-016-0245-4

Russell, C. T., Anderson, B. J., Baumjohann, W., Bromund, K. R., Dearborn, D., Fischer, D., Le, G., Leinweber, H. K., Leneman, D., … Richter, I. (2016). The magnetospheric multiscale magnetometers. *Space Sci. Rev.*, *199*(1–4), 189–256. https://doi.org/10.1007/s11214-014-0057-3

Sahraoui, F., Goldstein, M. L., Robert, P., and Khotyaintsev, Y. V. (2009). Evidence of a cascade and dissipation of solar-wind turbulence at the electron gyroscale. *Phys. Rev. Lett.*, *102*(23), 231102. https://doi.org/10.1103/PhysRevLett.102.231102

Shi, Q. Q., Yao, S. T., Hamrin, M., and Liu, J. (2024). Kinetic scale magnetic holes in the terrestrial magnetosheath: A review. *Sci. China Earth Sci.*, *67*(9), 2739–2771. https://doi.org/10.1007/s11430-023-1290-8

Stawarz, J. E., Eastwood, J. P., Phan, T. D., Gingell, I. L., Pyakurel, P. S., Shay, M. A., Robertson, S. L., Russell, C. T., and Le Contel, O. (2022). Turbulence-driven magnetic reconnection and the magnetic correlation length: Observations from magnetospheric multiscale in Earth's magnetosheath. *Phys. Plasmas*, *29*(1), 012302. https://doi.org/10.1063/5.0071106

Steinvall, K., Richard, L., Fülöp, T., Hanebring, L., and Pusztai, I. (2025). Eulerian and Lagrangian electron energisation during magnetic reconnection. *J. Plasma Phys.*, *91*(3), E90. https://doi.org/10.1017/S0022377825100408

TenBarge, J. M., Juno, J., and Howes, G. G. (2024). Electron energization in reconnection: Eulerian vs Lagrangian perspectives. *Phys. Plasmas*, *31*(2), 022901. https://doi.org/10.1063/5.0184710

Vech, D., Klein, K. G., and Kasper, J. C. (2017). Nature of stochastic ion heating in the solar wind: Testing the dependence on plasma beta and turbulence amplitude. *Astrophys. J. Lett.*, *850*(1), L11. https://doi.org/10.3847/2041-8213/aa9887

Vörös, Z., Yordanova, E., Varsani, A., Genestreti, K. J., Khotyaintsev, Y. V., Li, W., Graham, D. B., Norgren, C., Nakamura, R., … Saito, Y. (2017). MMS observation of magnetic reconnection in the turbulent magnetosheath. *J. Geophys. Res.: Space Phys.*, *122*(11), 11442–11467. https://doi.org/10.1002/2017JA024535

Wang, Y. W., Bandyopadhyay, R., Chhiber, R., Matthaeus, W. H., Chasapis, A., Yang, Y., Wilder, V., Gershman, D. J., Giles, B. L., … Burch, J. L. (2021). Statistical survey of collisionless dissipation in the terrestrial magnetosheath. *J. Geophys. Res.: Space Phys.*, *126*(6), e2020JA029000. https://doi.org/10.1029/2020JA029000

Xie, Z. K., Zong, Q. G., Yue, C., Zhou, X. Z., Liu, Z. Y., He, J. S., Hao, Y. X., Ng, C. S., Zhang, H., … Lindqvist, P. A. (2024). Electron scale coherent structure as micro accelerator in the Earth's magnetosheath. *Nat. Commun.*, *15*(1), 886. https://doi.org/10.1038/s41467-024-45040-5

Xu, Q. Y., Zhou, M., Ma, W. Q., He, J. S., Huang, S. Y., Zhong, Z. H., Pang, Y., and Deng, X. H. (2023). Electron heating in magnetosheath turbulence: Dominant role of the parallel electric field within coherent structures. *Geophys. Res. Lett.*, *50*(6), e2022GL102523. https://doi.org/10.1029/2022GL102523

Yang, Y., Matthaeus, W. H., Parashar, T. N., Haggerty, C. C., Roytershteyn, V., Daughton, W., Wan, M. P., Shi, Y. P., and Chen, S. Y. (2017). Energy transfer, pressure tensor, and heating of kinetic plasma. *Phys. Plasmas*, *24*(7), 072306. https://doi.org/10.1063/1.4990421

Yang, Y., Matthaeus, W. H., Roy, S., Roytershteyn, V., Parashar, T. N., Bandyopadhyay, R., and Wan, M. P. (2022). Pressure–strain interaction as the energy dissipation estimate in collisionless plasma. *Astrophys. J.*, *929*(2), 142. https://doi.org/10.3847/1538-4357/ac5d3e

Yang, Y., Pecora, F., Matthaeus, W. H., Roy, S., Cuesta, M. E., Chasapis, A., Parashar, T., Bandyopadhyay, R., Gershman, D. J., … Burch, J. L. (2023). Quantifying the agyrotropy of proton and electron heating in turbulent plasmas. *Astrophys. J.*, *944*(2), 148. https://doi.org/10.3847/1538-4357/acb25a

Yang, Y., Matthaeus, W. H., Oughton, S., Bandyopadhyay, R., Pecora, F., Parashar, T. N., Roytershteyn, V., Chasapis, A., and Shay, M. A. (2024). Effective viscosity, resistivity, and Reynolds number in weakly collisional plasma turbulence. *Mon. Not. R. Astron. Soc.*, *528*(4), 6119–6128. https://doi.org/10.1093/mnras/stae355

Yao, S. T., Wang, X. G., Shi, Q. Q., Pitkänen, T., Hamrin, M., Yao, Z. H., Li, Z. Y., Ji, X. F., De Spiegeleer, A., … Liu, J. (2017). Observations of kinetic-size magnetic holes in the magnetosheath. *J. Geophys. Res.: Space Phys.*, *122*(2), 1990–2000. https://doi.org/10.1002/2016JA023858

Yao, S. T., Shi, Q. Q., Guo, R. L., Yao, Z. H., Fu, H. S., Degeling, A. W., Zong, Q. G., Wang, X. G., Russell, C. T., … Giles, B. L. (2020). Kinetic-scale flux rope in the magnetosheath boundary layer. *Astrophys. J.*, *897*(2), 137. https://doi.org/10.3847/1538-4357/ab9620

Yao, S., Yue, Z., Shi, Q., William Degeling, A., Fu, H., Tian, A., Zhang, H., Vu, A., Guo, R., … Sun, W. (2021). Statistical properties of kinetic-scale magnetic holes in terrestrial space. *Earth Planet. Phys.*, *5*(1), 63–72. https://doi.org/10.26464/epp2021011

Yoon, Y. D., and Bellan, P. M. (2019). Kinetic verification of the stochastic ion heating mechanism in collisionless magnetic reconnection. *Astrophys. J. Lett.*, *887*(2), L29. https://doi.org/10.3847/2041-8213/ab5b0a

Yordanova, E., Vörös, Z., Raptis, S., and Karlsson, T. (2020). Current sheet statistics in the magnetosheath. *Front. Astron. Space Sci.*, *7*, 2. https://doi.org/10.3389/fspas.2020.00002